46th AIAA/ASME/SAE/ASEE Joint Propulsion Conference & Exhibit
25 - 28 July 2010, Nashville, TN

AIAA 2010-6772

VASIMR® Performance Results

Leonard D. Cassady*, Benjamin W. Longmier†, Chris S. Olsen†, Maxwell G. Ballenger†, Greg E. McCaskill‡, Andrew V. Ilin§, Mark D. Carter¶, Tim W. Glover‖, Jared P. Squire** and Franklin R. Chang Díaz††

Ad Astra Rocket Company, 141 W. Bay Area Blvd, Houston, TX 77598, USA

Edgar A. Bering, III‡‡

University of Houston, Department of Physics, Houston, TX, 77204,USA

The performance of a 200 kW VASIMR® engine has been experimentally measured. The high-power design was developed to test critical technologies and to provide performance measurements at power levels, magnetic field strengths, and configurations applicable to a flight unit. The VX-200 demonstrated the capability to operate with a total of 200 kW DC power input into RF generators and coupled to the plasma for a short pulse - proving that the technology does function at high power. The first stage, or helicon stage, generated an argon plasma with a minimum cost to make the ions of 87 eV per ion at approximately 28 kW input power and 107 mg/s argon flow rate. An average ion kinetic energy of 12 eV with only the helicon powered was calculated from plasma flux and force measurements near the thruster exit. The second stage, or ion cyclotron heating (ICH) stage, was operated from zero to 81 kW with the helicon at a fixed power of approximately 28 kW. Extensive measurements of the plasma flux, momentum, and ion kinetic energy in the far-field plume with the ICH stage operating at approximately 135 kW demonstrated a half angle of 24 degrees for 90% of the momentum and 30 degrees for 90% of the plasma flux with the second stage operating. The thrust efficiency and specific impulse increased from approximately 10% and 800 s to 54% and 3500 s, respectively, with increasing ICH power. The data show no saturation in the process that converts ion cyclotron frequency RF waves into ion energy. A semi-empirical model of the efficiency as a function of specific impulse matches the trends of the experimental data and predicts approximately 64% thrust efficiency at 6000 s and 200 kW.

Nomenclature

Symbols

η_n	Nozzle efficiency [%]
η_T	Thruster efficiency [%]
η_B	Percent of second stage coupled RF power that becomes directed kinetic energy [%]
Γ	Total ion flux through the rocket [s^{-1}]
θ	Half angle of the plume divergence [degrees]
e	Electron charge [1.60×10^{-19} C]
E_1	Kinetic energy of ions exiting first stage [eV]

*Lead Project Engineer and AIAA Member
†Research Scientist
‡Senior RF Engineer
§Computational Research Lead
¶Director of Technology
‖Director of Development
**Director of Research
††President and CEO
‡‡Professor, Physics and ECE, 617 Science & Research Bldg 1, Associate Fellow

E_2	Ion kinetic energy due to second stage heating [eV]
E_i	Ionization cost of the helicon stage [eV]
F	Total force measured in the plume [N]
g	Acceleration of gravity [9.81 m s^{-2}]
I_{sp}	Specific Impulse [s]
$\dot{m}$	Propellant (Argon) mass flow rate [kg/s]
m_{Ar}	Mass of an argon atom [kg]
$P_{1,RF}$	RF power coupled to the plasma in the first stage [W]
$P_{2,RF}$	RF power coupled to the plasma in the second stage [W]
P_{jet}	Thruster jet power [W]

I. Introduction

High-power electric propulsion systems have the capability of reducing the propellant mass for heavy-payload orbit raising missions and cargo missions to the moon and can even reduce the trip time of piloted planetary missions.[1–6] The Variable Specific Impulse Magnetoplasma Rocket (VASIMR®), is one of the few electric propulsion devices capable of processing a great power densities (∼6 MW/m^2) with an expected long lifetime. A simplified concept is shown in figure 1. The advantages of the VASIMR® are high power, high specific impulse, constant power variable specific impulse, and potentially long lifetime due to the magnetic confinement of the plasma stream. The rocket relies on efficient plasma production in the first stage using a helicon plasma source.[7,8] Ion cyclotron resonance enables efficient ion heating in the second stage (RF booster). Thrust is realized in the final stage as the plasma accelerates in a magnetic nozzle. End-to-end testing of the VASIMR® with a spaceflight-like configuration, the optimum magnetic field configuration, and a vacuum facility large enough and with enough pumping to allow for plume measurements with low background pressure had not been achieved until recently.

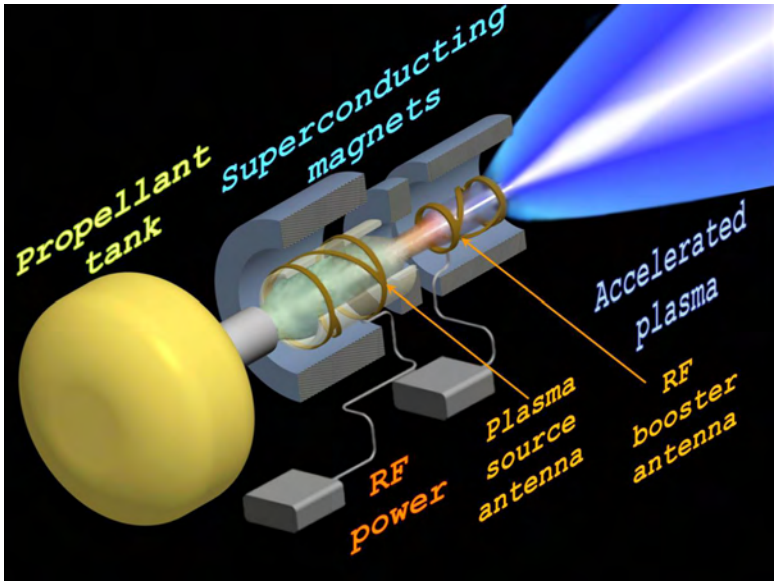

Figure 1. An image of the VASIMR® concept.

Ad Astra Rocket Company has been hard at work improving the VASIMR® design and plume diagnostics in order to measure rocket performance at 200 kW. Previous versions of the VASIMR® and limitations of the vacuum facility hindered the effort to accurately measure performance.[9–11] The most recent technical publications[12–15] do not show full power operation at 200 kW, nor was there enough plume data to calculate thrust efficiency.

In this paper we demonstrate that a VASIMR® in a configuration similar to a spaceflight design can operate at 200 kW and efficiently (greater than 50%) produce force in the specific impulse range of interest. This paper primarily presents experimental results recorded over the past year that benefit from a high-

quality vacuum facility with excellent plume diagnostics. Plasma flux, RF power measurements, and neutral argon gas flow rate measurements, combined with knowledge of the kinetic energy of the ions leaving the rocket are used to show ionization cost of the argon, force produced by the thruster, and the thrust efficiency. Here we present new experimental data that demonstrate performance above 100 kW, the best operating conditions for which measurements have been obtained.

We first present a description of the VX-200 and its vacuum facility in sections II and III. Next in section IV, we briefly discuss the 200 kW power milestone. The plasma diagnostics and improvements in VX-200 operation are presented in section V. The experimental results of ionization cost, plume expansion angle, thruster efficiency and force are presented in sections VI to VIII. A semi-empirical model of the thrust efficiency as a function of specific impulse is presented in section IX. Finally, the future application of the VASIMR® on the International Space Station (ISS) is discussed.

II. The VX-200

The VX-200 is an experimental version of the VASIMR® engine that is designed to utilize 200 kW of input DC electrical power. The experimental rocket is an end-to-end test of the primary components in a vacuum environment with the goal of measuring and improving performance. Most components of the rocket are located within the vacuum chamber, with only the RF generators, magnet power supplies, and magnet cryocoolers at atmospheric pressure outside of the vacuum chamber. The superconducting magnets, structural components, rocket core, and many electronic components are operated within the chamber. Figure 2 shows an image of the VX-200 3-D CAD model and a picture of the rocket installed inside the vacuum chamber. A key subsystem of the VX-200 is the superconducting magnet with a maximum field of approximately 2 Tesla that allows for efficient containment and acceleration of the plasma. Another key subsystem is the rocket core - the components that physically surround the plasma and intercept the bulk of the waste heat.

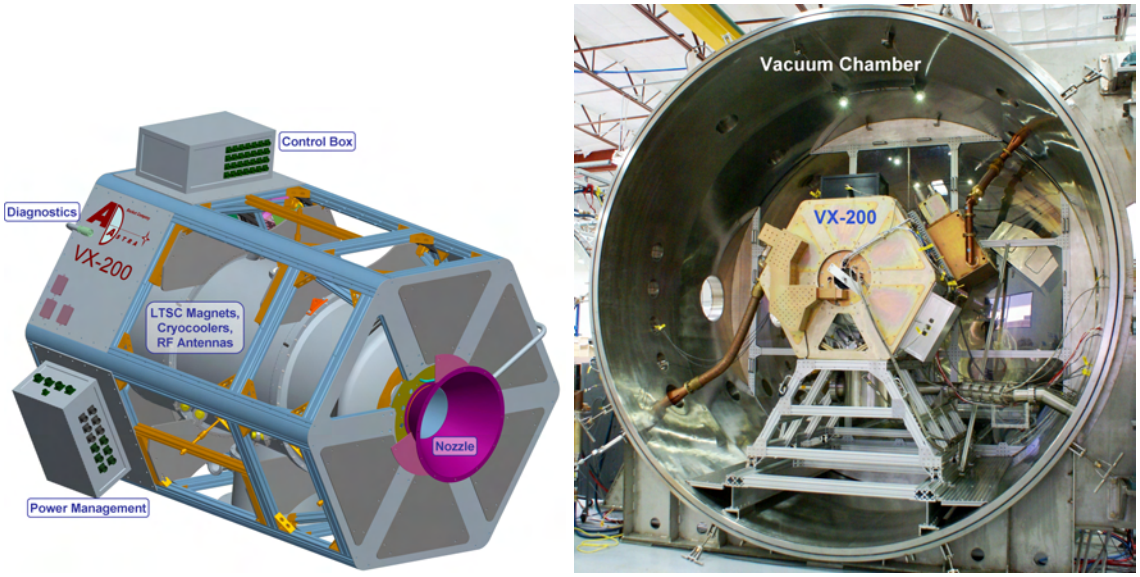

(a) An image of the simplified 3-D model of the VX-200 with a point of view from the aft end.

(b) A picture of VX-200 installed in the large chamber at Ad Astra Rocket Company.

Figure 2. Images of the VX-200.

The VX-200 is restricted to pulses of less than one minute in length owing to temperature limitations of certain seals and joints in the rocket core. We will use the thermal data gathered from the pulsed operation to design the optimal thermal solution for the measured heat flux in future models. Most VX-200 pulses are between 1 and 15 seconds in length.

The first stage, or helicon stage, launches a right-hand circularly polarized wave into the plasma. The plasma diameter is reduced by more than a factor of 2 as it flows downstream through a “magnetic choke”

and containment wall that follows the plasma flux tube. Up to 40 kW of RF power (RF generator limited) can be deposited into up to 150 mg/s of flowing argon plasma. The second stage, or Ion Cyclotron Heating (ICH) stage, couples energy directly into the ions via ion cyclotron resonance with a wave that is launched into the plasma via a specially designed, proprietary coupler. The exhaust velocity of the ions increases as the RF power that is coupled into the ICH section increases.

The primary components are the propellant flow controller, RF generators, rocket core, and magnet. Argon gas flow control is provided by a Moog flow controller that can supply up to 150 mg/s. The other two components are described in the following subsections.

A. RF Generators

The VX-200 utilizes two solid-state RF generators developed by Nautel Limited of Canada specifically for this application. The helicon section RF generator converts power supplied at 375 VDC into approximately the industrial standard of 6.78 MHz RF with an efficiency of greater than 92% at up to 40 kW. The specific mass of the helicon section RF generator is less than 1 kg/kW. The ICH section RF generator converts power supplied at 375 VDC into ∼500 kHz RF with an efficiency of greater than 98% at up to 170 kW. The specific mass of the ICH section RF generator is less than 0.5 kg/kW. These RF generators are not located within the vacuum chamber, but transmit the RF power into the vacuum chamber to the VX-200 through high-voltage, high-power RF feedthroughs. The components of the generators were not designed to operate in vacuum to ensure their availability for testing with the VX-200.

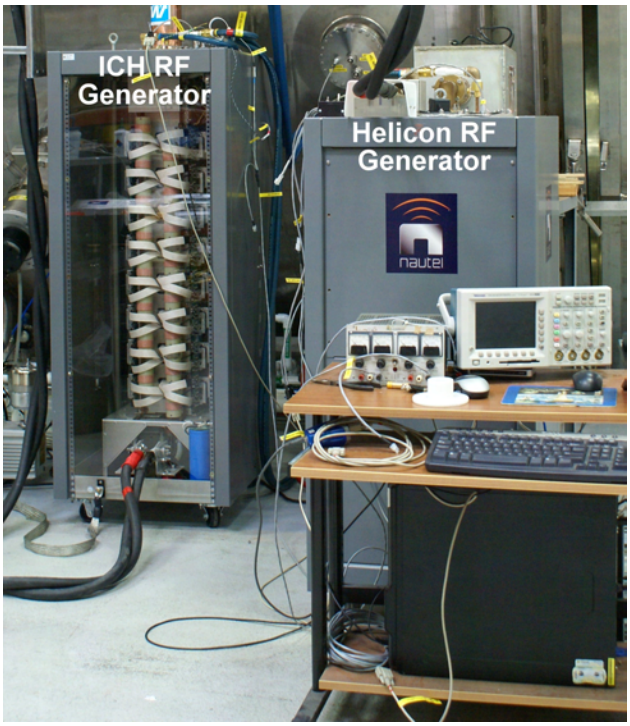

Figure 3. A picture of ICH RF generator and the helicon RF generator.

B. Low Temperature Superconducting Magnet

The VASIMR® relies on magnetic fields to limit plasma erosion of the surrounding materials as well as to provide the field strength necessary for ion cyclotron resonance at a frequency that does not excessively excite electrons and limits the cyclotron radius. The gyroradius should be much less than the plasma radius, which corresponds to a field strength of greater than 1 T. In order to have an efficient electric propulsion device, the magnet must consume a small amount of power compared to thrust power. The only feasible method to generate such a strong magnetic field in space is with a superconducting magnet. The VX-200 utilizes a state-of-the-art low temperature superconducting magnet designed and developed by Scientific Magnetics,

LLC of the United Kingdom specifically for the VX-200. The magnet is shown in figure 4. The spaceflight VASIMR® will utilize a high temperature superconducting magnet so that the heat-rejection systems that chill the magnet can operate at high efficiency.

Figure 4. A picture of the low temperature superconducting magnet with alignment fixtures mounted to the ends.

C. Rocket Core

The rocket core is the most critical subsystem of the VASIMR® as it must protect the first and second stage RF couplers from the plasma, allow the RF to transmit with low loss to the plasma from the couplers, conduct many kilowatts of heat away from the plasma facing walls and magnets, and survive for tens of thousands of hours. Presently, Ad Astra is testing various configurations of the core to measure heat flux from the plasma and to find the best materials and layouts for steady-state operation at full power.

III. Vacuum Facility

Ad Astra Rocket Company operates a stainless steel vacuum chamber (see figure 5) designed for testing the VASIMR® engine. The vacuum chamber is 4.2 m in diameter and 10 m long with a volume of 150 m^3 (including the end caps). One end opens fully for access to the entire inner diameter. The vacuum chamber is partitioned into two sections, a rocket section and an exhaust section. The rocket section stays at a lower pressure than the exhaust section while the VX-200 is firing. The partitioning was done to prevent arcing and glow discharges near the high voltage transmission lines and matching circuit components. There is a 2.5 m by 5 m translation stage that carries a suite of plasma diagnostics for plume characterization. The translation stage uses 2 independent ball screws and is driven by vacuum compatible stepper motors which yield a positional resolution of 0.5 mm. The facility has the capability of pumping 200,000 liters/s argon and 300,000 liters/s nitrogen with four PHPK Technologies CVI Torr Master® internal cryopumps. Presently, only two pumps are being operated which reduces the pumping speed by a factor of two. The exhaust section pressure is low enough (less than 1×10^{-5} torr) for the first 0.8 s of operation that collisions with background neutral gas do not affect the results. The pressure is less than 1×10^{-7} torr before each shot. The pressure rises to a maximum of 2×10^{-4} torr after the rocket has been operating for more than 0.8 s.

Figure 5. A picture of the "El Monstro" large vacuum chamber at Ad Astra Rocket Company.

IV. 200 kW Milestone

One of the primary goals of the VX-200 was to demonstrate the efficient conversion of 200 kW of DC electrical power into thrust. We have separately demonstrated the ability to process 200 kW of power and the efficient conversion of that power into thrust. In September of 2009, the VX-200 operated with 200 kW input power for approximately 0.1 s, as shown in figure 6. This was an important milestone demonstrating hardware capable of operating in vacuum at full power. The second stage coupler used for the full-power demonstration was a first generation design that was not optimized for efficient ion acceleration. We are presently testing different couplers to operate at full power and high efficiency. In the following sections we will present measurements that demonstrate efficient operation at derated power.

V. Plume Measurements and Plasma Pulses

Plasma flux measurements are performed using a planar molybdenum 10-collector Langmuir probe array biased into ion saturation and mounted on the translation stage. A fixed 70 GHz microwave interferometer measures the electron density at the VX-200 exit. However, the electron density for the data presented here were too high for the frequency of this system to measure a quantity. To determine a quantity for thrust, we rely on a force target technique that has been validated against a Hall thruster on a thrust stand.[16] The force target is a graphite disk mounted to a sensitive strain gauge and scanned across the plasma profile to integrate a total force. Gridded Retarding Potential Analyzers (RPA) are also installed on the translation stage to measure ion energy, and combined with the flux, independently predicts a thrust value for cross checking with the target. Spatial data are collected both by moving the translation stage shot-to-shot for short pulses and moving the translation stage during extended pulses. The diagnostics mounted on the top of the translation stage are shown in figure 7.

In order to accommodate advances in low-mass solid-state RF power generation in anticipation for space-flight, new proprietary algorithms had to be developed for successful high-power startup. Some of the first recipes involved active tuning of the RF circuit over several seconds before acceptable helicon modes were

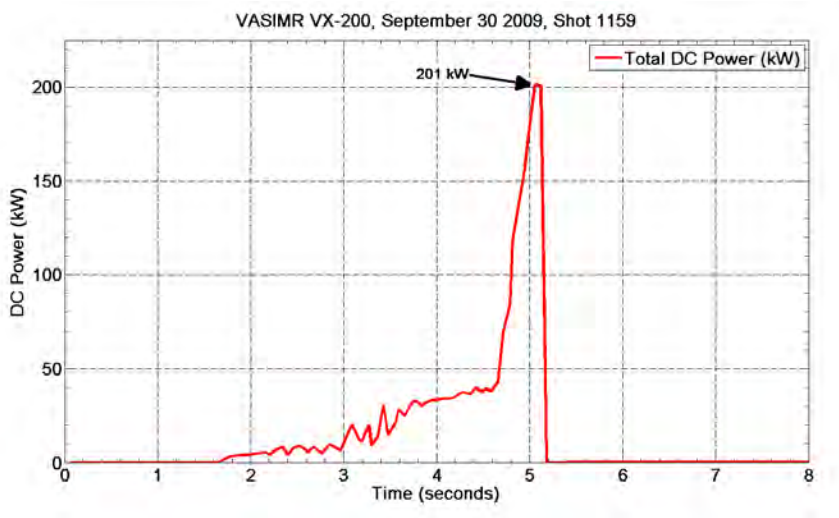

Figure 6. A graph of the input electrical power as a function of time for the 200 kW milestone.

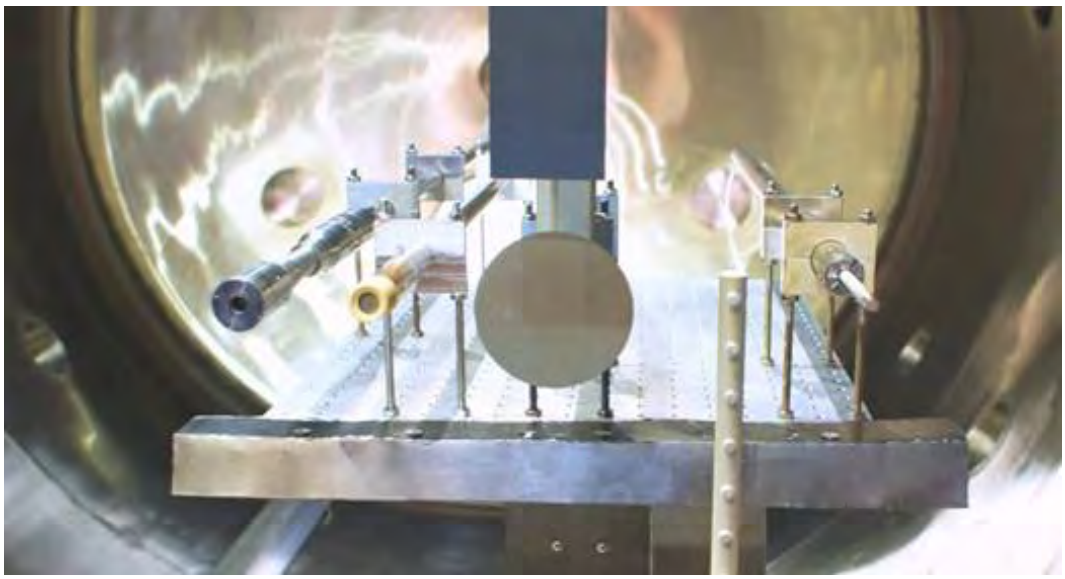

Figure 7. A picture of the diagnostics mounted to the translation stage.

achieved (figure 8a). These methods recently have been drastically improved resulting in fast (<100 ms) coupling of the helicon mode into the plasma (figure 8b). Improvements can still be made, however, neutral gas dynamics will ultimately limit the startup time when the distance between the fuel reservoir and ionization chamber must be taken into account.

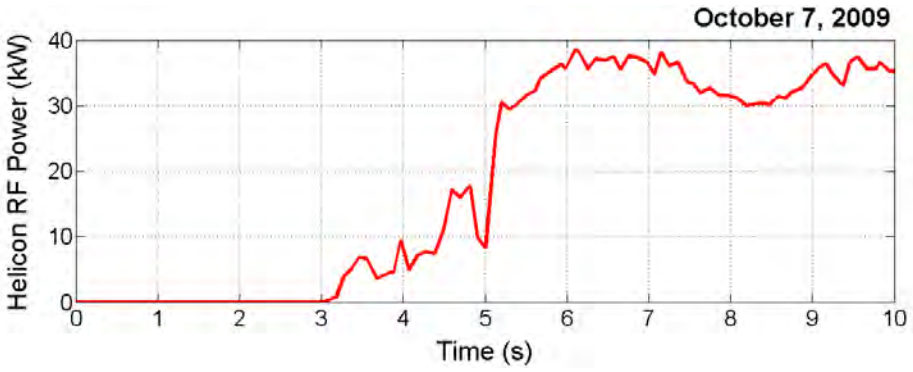

(a) Helicon RF power startup temporal profile with active tuning.

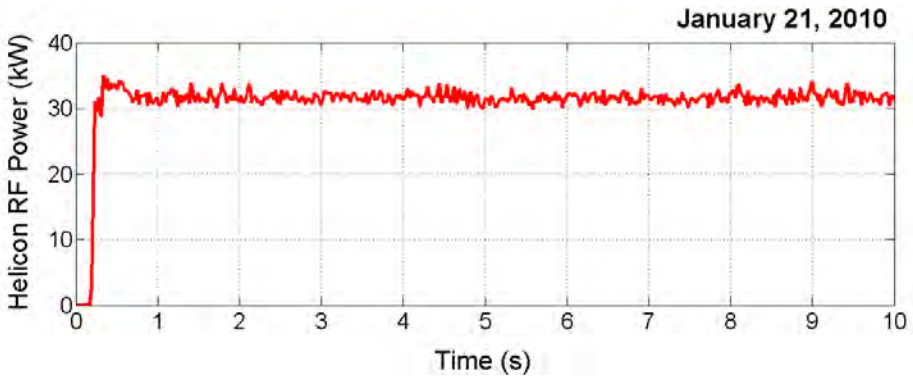

(b) Helicon RF power startup temporal profile with advanced tuning.

Figure 8. Comparison of the time for the helicon to reach steady state operation.

A. Flux Probes

Measurements of the ion flux presented in this paper were taken with an array of ten 0.25 inch diameter molybdenum planar probes of a top hat design[17] that were biased into the ion saturation regime, -15 V with respect to chamber ground, during VX-200 operation. Occasionally, full I-V traces were taken and analyzed so that we could be sure that the probes were properly biased. Ion flux measurements were taken both during quick startup shots, where the ambient neutral gas pressure was below 1×10^{-5} Torr, and during translating radial profiles where the sustained neutral argon pressure within the vacuum chamber was below 2×10^{-4}.

B. Force Target Construction and Operation

The force target, described in detail in an earlier publication,[16] consists of a 9-centimeter-diameter graphite target disc attached to a 10-centimeter-long insulating alumina rod. The stiff alumina rod then connects to a small titanium bar (5.72 cm $\times$ 1.30 cm) where a series of 4 high output semiconductor strain gauges, Micron Instruments model number SS-090-060-1150P, are mounted between two holes on an "isthmus" on the titanium bar, as seen in figure 9, similar in design to earlier concepts.[18] The isthmus acts as a stress concentrator and increases the sensitivity of the device. The strain gauges are connected electrically in a Wheatstone bridge configuration so that changes in temperature of the titanium bar do not affect the linearity of the strain gauge output.

When the electrically floating graphite disc is immersed in flowing plasma (e.g. the plume of the VX-200) the force from the plasma impacting the graphite target is translated into a strain in the titanium beam through a moment arm equal to the length of the alumina rod plus the clamp length. A small graphite shield was also used to keep the entire titanium bar and strain gauge assembly shielded from the flowing plasma, and associated thermal and electrical noise.

The resolution of the force target is 0.1 mN, which allowed for sufficiently sensitive measurements of the force applied by the exhaust plasma. The natural frequency of oscillations was 40 Hz, and this oscillation is filtered out during the analysis of radial or temporal force profiles, though the temporal data is limited in resolution to 1/40 s.

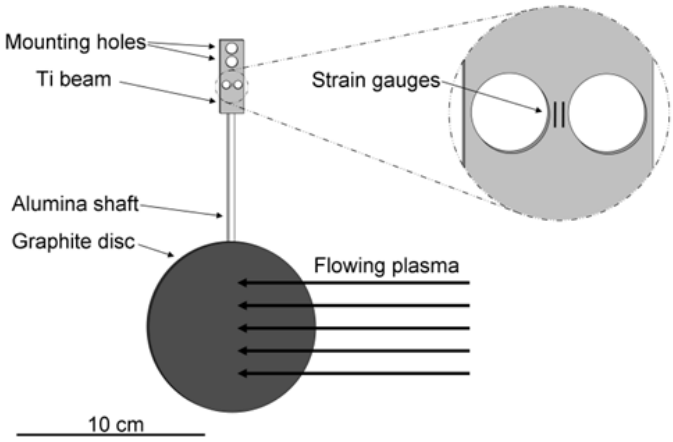

Figure 9. A schematic of the force target assembly and magnification of strain gauge arrangement mounted on the titanium isthmus.

C. Retarding Potential Analyzer

Retarding potential analyzer (RPA) diagnostics have been installed to measure the accelerated ions. Measurements of the ion energy in the exhaust of the VX-200 plume were made with a cylindrical 4x 2-layer grid RPA mounted on powered goniometric hinge on the translation stage, to enable pitch angle scans. A four-grid configuration is used, with entrance attenuator, electron suppressor, ion analyzer and secondary suppressor grids. The grids were 49.2-wire/cm molybdenum mesh, spaced 1 mm apart with Macor spacers. The opening aperture is 1 cm in diameter, usually pointed at the plasma beam.

The ion exhaust parameters are deduced from the raw data by means of least squares fits of drifting Maxwellians to the current-voltage data. The RPA I-V characteristic data has been reduced by least-squares fitting of the characteristic that would be produced by a drifting Maxwellian to the data. The three free parameters in these fits are ion density, mean drift speed and the parallel ion temperature in the frame of reference moving with the beam. The temperature is found from these least squares fits, not from taking the slope of the logarithm of the data. The temperature and ion drift speed parameters depend most strongly on the accuracy with which the retarding potential is known. The absolute uncertainty of the sweep voltage digitization with respect to chamber ground was a few percent when digitizer calibration uncertainty, sweep isolator reduction ratio precision and related parameters are folded in.

VI. Measurement of Ionization Cost

A key factor in maximizing the overall rocket efficiency is to create the plasma in the first stage with as little power as possible. The commonly used term for plasma generation efficiency is ionization cost and is presented as energy per ion in terms of electron volts. The VASIMR® helicon section has argon input into the upstream end and it flows to the ICH section. The RF power strips one electron off each ion. Power is lost through radiation from the excited argon neutrals and ions, flux of plasma to the walls where it recombines, and the frozen flow loss of ionization energy carried out of the helicon section. The ions also carry kinetic energy, E_1, but we do not count that as a loss since that energy represents thrust. Therefore the ionization cost is

$$E_i = \frac{P_{1,RF}}{\frac{\dot{m}}{m_{Ar}}} - E_1. \tag{1}$$

New measurements of the ionization cost were taken during helicon-only operation as a function of both RF power and argon propellant flow rate within the ranges of 15 to 35 kW and 50 to 150 mg/s, respectively. Ionization cost was determined by measuring the total ion flux from the VX-200 and then dividing the coupled RF power to the plasma by the total flux. Figure 10 is a contour map of the helicon performance as

an ion source, and shows a clear indication of a valley of optimum ionization cost, as low as 87 ± 9 eV per ion. Of course, each new core and helicon coupler will produce a unique ion cost performance map, though in general it is clear that providing too much propellant with too little RF power will result in an inefficient helicon plasma source. A scenario where there is too little propellant and too much RF power will also result in an inefficient helicon plasma source, though this region was out of range for the current setup because the plasma load changed too much for the matching circuit to compensate. Future experiment campaigns will look at constant power throttling of the VX-200, and this performance map provides a starting point for the operational settings of the helicon stage. A key point to remember with these ionization cost measurements is that this is the cost of an ion that is actually extracted all the way through the rocket core, which is in many cases quite different from the ion cost directly within a helicon source tube as reported by many other university labs. The lowest ionization cost measurement of 87 ± 9 eV occurred with VX-200 settings of 28 kW and 130 mg/s. Figure 11 shows the lowest ion cost measurements for each particular RF power setting, for which the flow rate is not fixed.

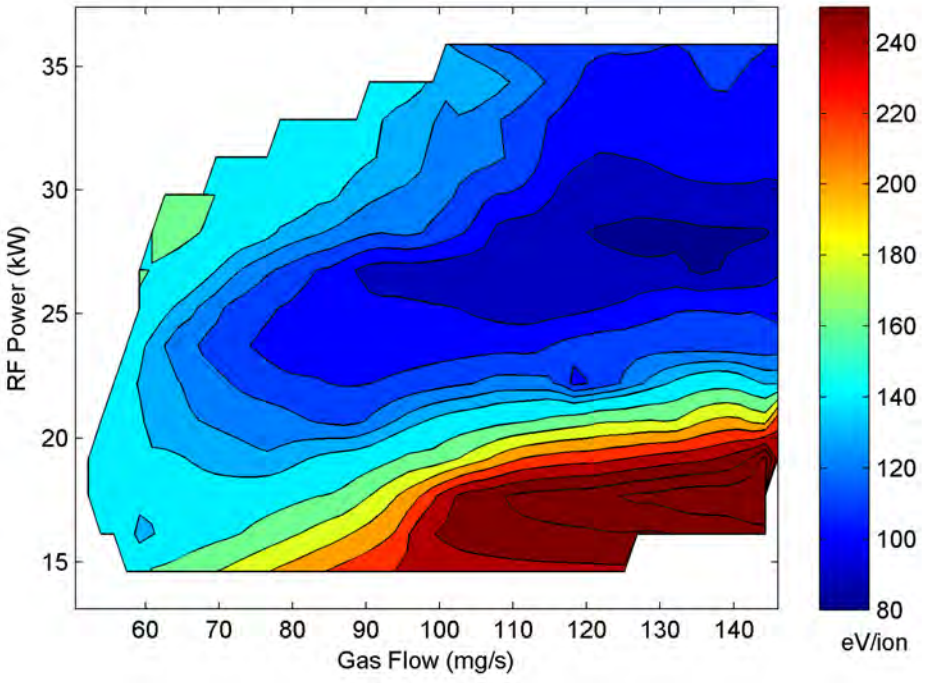

Figure 10. A color contour plot of the ionization cost of the helicon stage as a function of both RF power and argon gas flow rate. The uncertainty of the ionization cost is 10%.

Exiting parallel ion energy for helicon-only operation was determined by using the measured total force and the measured total ionization fraction. The ionization fraction was determined by the ratio of the total measured ion current to that of the measured input propellant flow rate by a mass flow controller. During normal operation of the helicon source at 28 kW and 107 mg/s of argon flow, the measured ionization fraction within the exhaust plume, 40 cm downstream from the VX-200, was $95\% \pm 5\%$. Together with a total force measurement and a total coupled RF power measurement, a 95% ionization fraction yields an average parallel (axial) ion energy of 12 ± 1 eV. This energy that the ions gain is likely due to an ambipolar ion acceleration process[19] as a result the expanding geometry of the magnetic field and a conversion of electron temperature into directed ion kinetic energy through a large scale axial electric field. No double layer structures were observed. We speculate that double layer structures require a much higher neutral gas pressure and, hence, the presence of a downstream plasma source within the vacuum chamber. The neutral gas pressure during the flux measurements was held below 1×10^{-5} torr. It should also be noted that all plasma facing components within the VX-200 are electrically floating, an important distinction when discussing ion energy values with a thruster in a grounded chamber. Radial flux maps, figure 12a, and radial force maps, figure 12b, give an indication of the ion energy distribution as a function of radial location in the exhaust plume. In fact, the ion energy distribution is relatively flat across the diameter of the exhaust

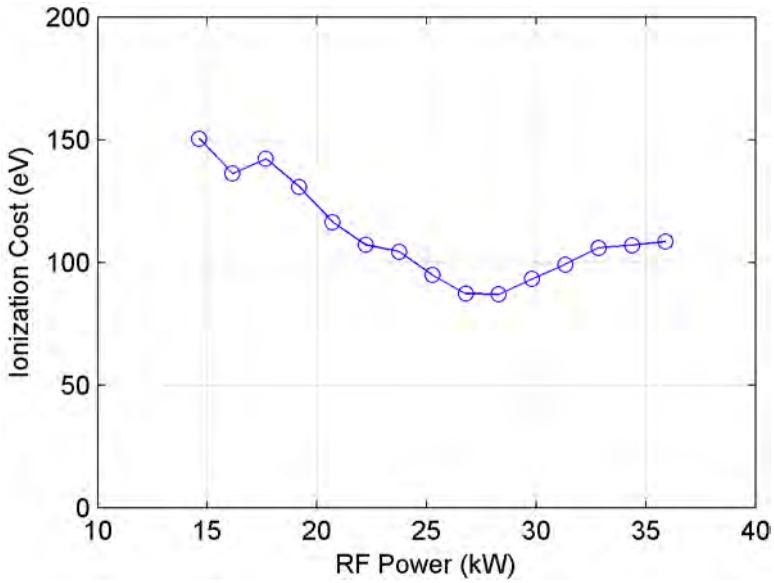

Figure 11. The minimum ionization cost as a function of helicon RF coupled power. The uncertainty of the ionization cost is 10%.

plume.[11]

VII. Plume Expansion Angle and Nozzle Efficiency

We have mapped the plasma flux density and force density over a large distance, further than 2 m from the VX-200 exhaust exit. This mapping was done with an earlier, less efficient VX-200 configuration, with a total power of 165±5 kW and a moderate neutral background pressure ($\sim 10^{-4}$ torr). Nevertheless, this is our best available data to date for determining plume expansion and estimating the nozzle efficiency. This was acquired over many plasma pulses by moving the diagnostics on the translation stage shot-to-shot. Even though the charge exchange mean free path was quite short (~ 0.1 m), the plasma jet data exhibit a well defined edge in both flux and force density. Figure 13 contains contour plots of that data. By assuming axial symmetry, we calculate the boundary contour that surrounds 90% of the integrated respective density. The angle of that boundary line relative to the axis, θ, is an estimate the exhaust divergence angle. Lines drawn on the figures represent the estimated angles. The flux data show an angle of 30 degrees, while the force density data show 24 degrees. We expect that the difference in the angles is due to interaction with the background neutral density through charge exchange collisions and the flux density divergence represents a worse case. The momentum direction of the plasma jet is mostly conserved with charge exchange, so the force density divergence represents the best case. From these angles, we estimate the nozzle efficiency using the classic nozzle formula

$$\eta_n = \frac{1}{2}(1 + \cos\theta). \tag{2}$$

We find that the nozzle efficiency is at least 93% and as high as 96%. For the following system efficiency analysis, we'll use the more conservative 93% nozzle efficiency. This estimate is consistent with particle trajectory modeling[20] that predicts a nozzle efficiency of 93%. Calculations based on a robust MHD theory[21] that factors in possible drag effects due to the plasma leaving the high magnetic strength zone give a nozzle efficiency of 87%. The high charge exchange conditions of the present data do not allow us to test the MHD theory yet. We plan to soon perform such measurements with charge exchange mean free paths exceeding 1 meter, so the long range magnetic effects may be observed.

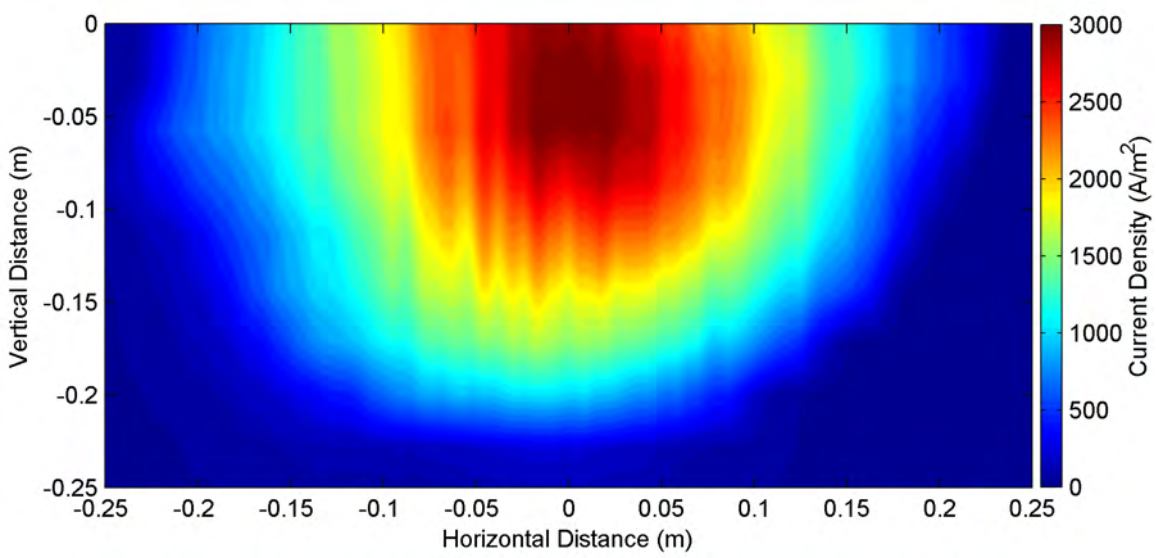

(a) Current density map for helicon-only operation. The axis are relative to the axis of the rocket. The flux density peak is slightly off-center, probably due to the diagnostic translation stage blocking a fraction of the plume below axis.

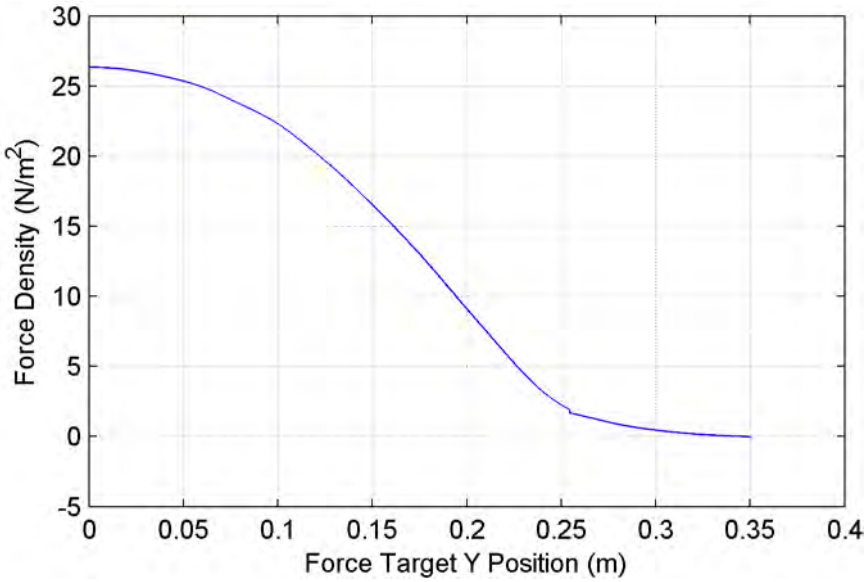

(b) A horizontal force density profile.

Figure 12. Force profile and current density map of helicon operation. The ionization cost is determined from the flux and input RF power. The energy in the ions determined from the force.

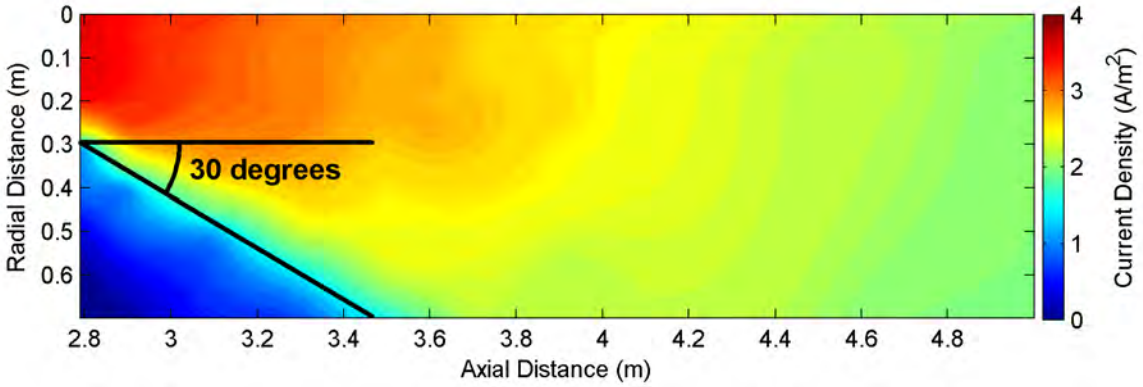

(a) Contour plot of the current density with a total RF power of 165 kW. The half-angle of 30 degrees within which 90% flux is contained is shown.

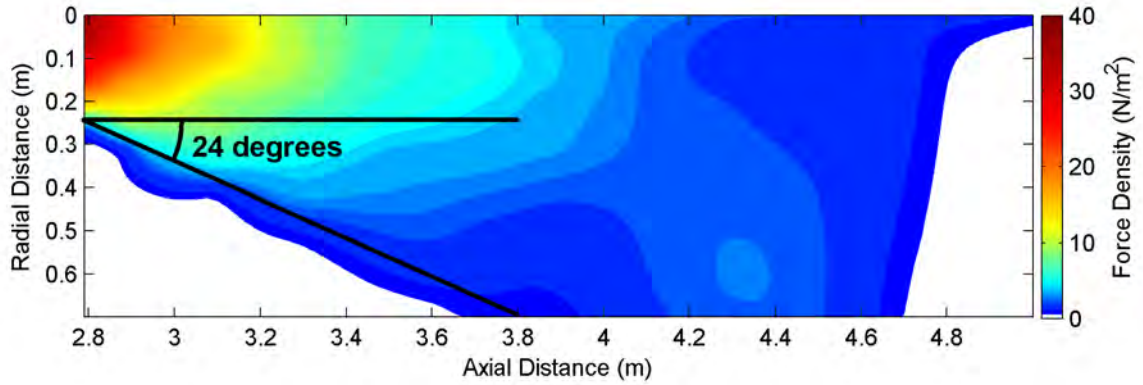

(b) Contour plot of the force density with a total RF power of 165 kW. The half-angle of 24 degrees within which 90% momentum is contained is shown.

Figure 13. Contour plots of the force density and flux density in the near-field and far-field plume of the VX-200 with 162 kW of total input power.

VIII. Thruster Efficiency and Force

The VX-200 thruster efficiency is determined by dividing the total RF power coupled to plasma by the thruster jet power. The jet power is defined as

$$P_{jet} = \frac{F^2}{2\dot{m}}, \tag{3}$$

where F is the total force produced by the rocket and $\dot{m}$ is the total mass flow rate of propellant. The force from VX-200 was determined by by using a force impact target that measured the local force density within the exhaust plume as a function of radial position. The force density over one full diameter of the exhaust plume was integrated, with the assumption of azimuthal symmetry, in order to determine the total force produced by the VX-200. The force density diameter profile was taken 40 cm downstream from the end of the VX-200 thruster. This force measurement location is approximately 30 cm downstream of the magnetic nozzle, where the end of the magnetic nozzle is defined as the point where 90% of the perpendicular ion momentum has been converted to parallel momentum along the axis of the thruster, a process described by conservation of the first adiabatic invariant. The force target is 9 cm in diameter, small compared to the total exhaust plume diameter of approximately 50 cm, and has a resolution of 0.1 mN. Dividing equation 3, by the total RF power coupled to the plasma gives

$$\eta_T = \frac{P_{jet}}{P_{1,RF} + P_{2,RF}}, \tag{4}$$

where $P_{1,RF}$ and $P_{2,RF}$ represent the RF power coupled to the first and second stage plasma, respectively.

An experiment campaign in May of 2010 that used a propellant flow rate of 107 mg/s yielded results that show a total force of up to 3.6 N and 54% efficiency at a total coupled RF power of 108 kW. The specific impulse was calculated using the total force measurement and a propellant mass flow rate measurement where

$$I_{sp} = \frac{F}{\dot{m}g}. \tag{5}$$

Figure 14a shows the force as a function of I_{sp}. Figure 14b shows the VX-200 thruster efficiency as a function of the total RF power coupled to the plasma. The Helicon stage is left at a constant 28 kW, while the ICH stage power is varied from 0 to 81 kW. The limiting factor in the maximum applied RF power to the VX-200 in this experiment campaign was a vacuum pressure limit within the vacuum chamber, where greater RF circuit voltages produced glow or arc discharges which prompted the solid state RF generators to shut down. Standard high voltage conditioning techniques are used to mitigate these risks and a push for higher power levels at lower pressure is forthcoming in future experiment campaigns. The efficiency continues to increase as a function of applied ICH RF power, indicating that the process of ICH wave coupling into the plasma column has not saturated.

Figure 15 shows the same data set from May 2010 but displays the thruster efficiency of the VX-200 as a function of the specific impulse of VX-200. The relation between efficiency and specific impulse is an important design metric that we have been working to measure. We are extremely satisfied with greater than 50% efficiency at as low as 3000 s I_{sp} for this experimental device. A semi-empirical model is also graphed in figure 15, and is a least squares fit the to the data using ICH coupling efficiency as a free parameter. The free and fixed (measured) parameters of the model are explained in the following section.

Retarding potential energy analyzer data taken during the campaign corroborates the determined ion energy to within 10% at high ICH power levels. Figure 16 shows a comparison of contour plots of the 2-D ion velocity phase space distribution function for ICH on vs ICH off. These data were obtained 2 m downstream from the ICH resonance. The measurements were made using the powered angle scan mount of the RPA, moving the translation stage so as to keep the RPA in one place. These figures show two things. First, the accelerated ion jet is tightly collimated in velocity space. Second, at this distance, the unaccelerated component shows evidence of a substantial amount of elastic scattering to higher pitch angles. Figure 14b also indicates that the ICH wave coupling process is not saturated, as the efficiency of the VX-200 continues to increase with increasing applied ICH power. The VX-200 helicon and ICH couplers were designed to produce a thrust efficiency of 60% at 5000 s, and the data indicate that the VX-200 is more efficient than the original design goal.

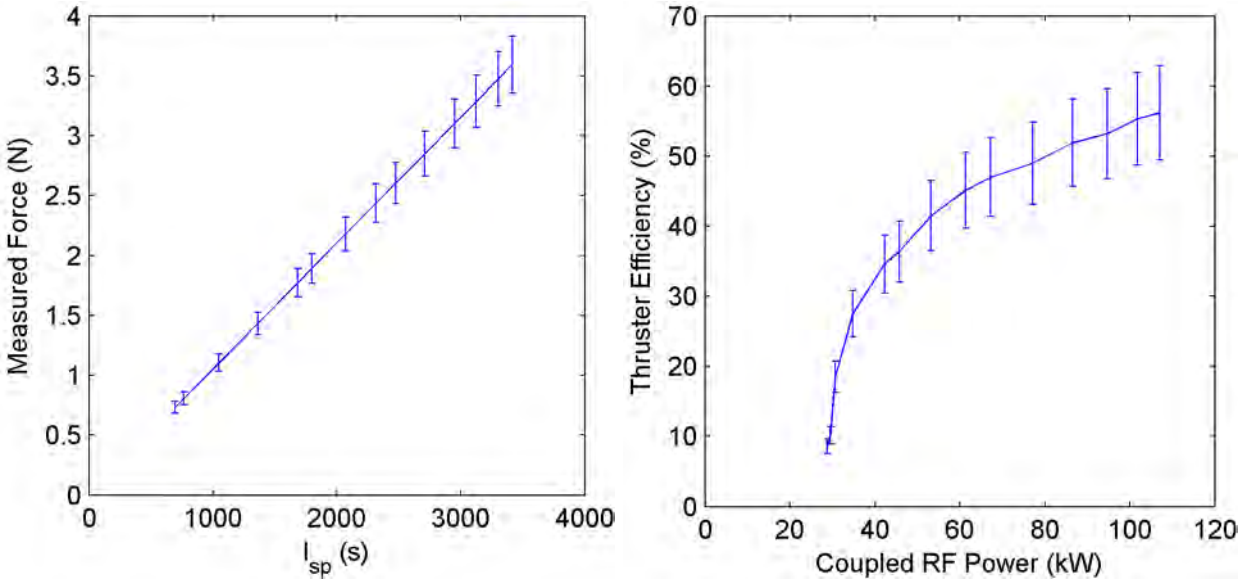

(a) The total VX-200 force as a function of specific impulse.

(b) The VX-200 thruster efficiency as a function of coupled RF power.

Figure 14. Force and efficiency measurements with the helicon stage fixed at 28 kW and the ICH power varied between 0 and 81 kW.

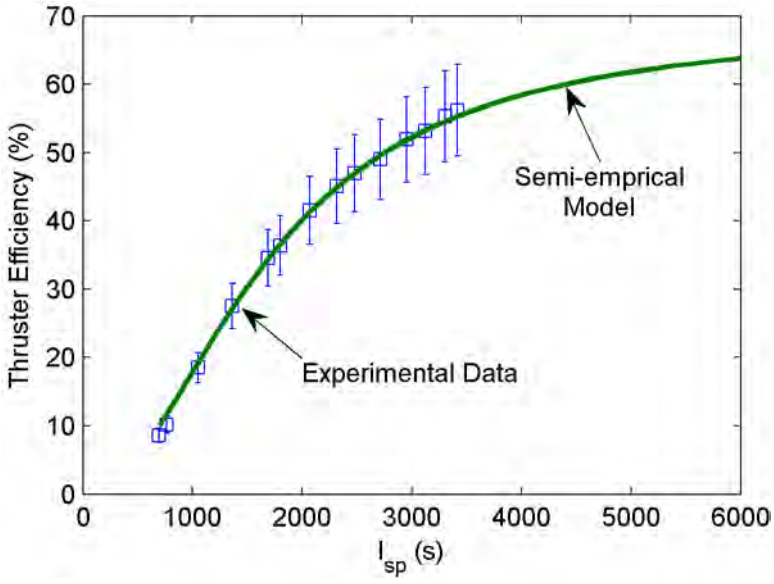

Figure 15. Measured efficiency data compared to semi-empirical model.

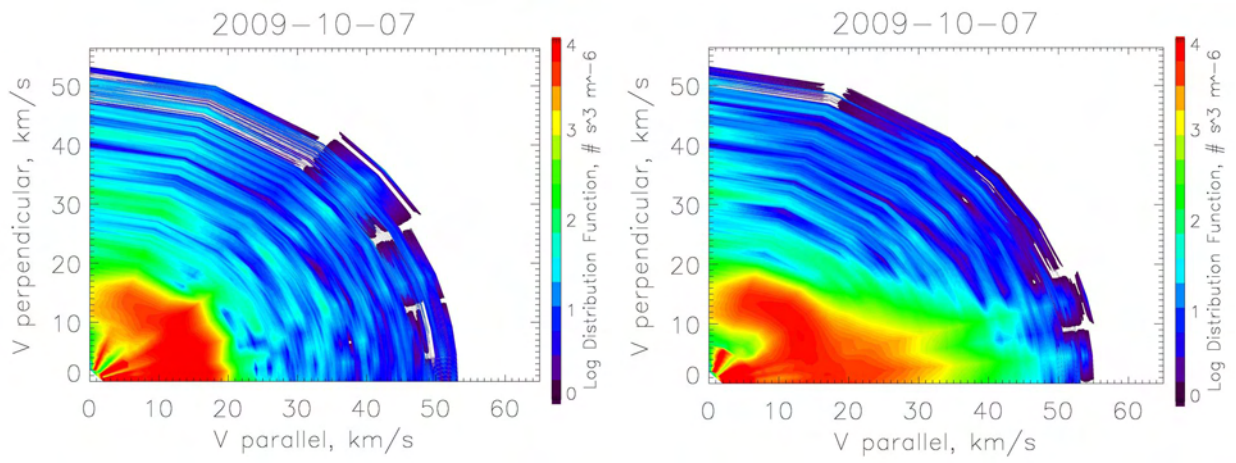

(a) Helicon only operation.

(b) Helicon and ICH operation.

Figure 16. Ion velocity phase space distribution function measured on axis 2 m downstream of the VX-200 exit.

IX. Efficiency Model

We have developed a thrust efficiency model for the VASIMR® engine based on the efficiencies of the major processes. The thrust efficiency, η_T, includes only the input RF power coupled to the plasma, not RF power lost in the transmission lines, matching networks, or within the RF generators themselves. Generating the plasma in the first stage is one of the primary energy losses, where most of the RF power ends up in the plasma containment walls via radiation or direct bombardment. The plasma leaving the first stage also carries with it directed kinetic energy, E_1, that produces thrust and is also expressed as eV. The RF power in the first stage, $P_{1,RF}$, is

$$P_{1,RF} = e\Gamma(E_i + E_1), \tag{6}$$

where e is the electron charge and Γ is the total ion flux in particles per second. The second stage coupler does not couple all of the RF power to the ion cyclotron motion of the ions - some energy is lost to electrons, ion thermal modes, metastable ions and radiation. The second stage RF power coupled to the ions that is converted into directed kinetic energy, E_2, is related to second stage RF power by the relation

$$P_{2,RF} = \frac{1}{\eta_B} e\Gamma E_2, \tag{7}$$

where η_B is the efficiency of coupling RF power to kinetic energy. The jet power, P_{jet}, is related to the sum of the ion directed kinetic energies multiplied by the nozzle efficiency, η_n,

$$P_{jet} = \frac{1}{2}\Gamma m_{Ar} g^2 I_{sp}^2 = e\Gamma(E_1 + E_2)\eta_n, \tag{8}$$

where g is the acceleration of gravity, and I_{sp} is the specific impulse. Using the relation for jet power we can express E_2 as a function of E_1 and I_{sp}

$$E_2 = \frac{\frac{1}{2} m_{Ar} g^2 I_{sp}^2}{e\eta_n} - E_1. \tag{9}$$

Writing the thrust efficiency as

$$\eta_T = \frac{P_{jet}}{P_{1,RF} + P_{2,RF}} = \frac{\frac{1}{2}\Gamma m_{Ar} g^2 I_{sp}^2}{e\Gamma E_i + e\Gamma E_1 + \frac{1}{\eta_B} e\Gamma E_2} \tag{10}$$

and substituting for E_2 using equation 9 gives efficiency as a function of I_{sp}

$$\eta_T = \frac{\frac{1}{2} m_{Ar} g^2 I_{sp}^2}{eE_i + eE_1(1 - \frac{1}{\eta_B}) + \frac{\frac{1}{2} m_{Ar} g^2 I_{sp}^2}{\eta_B \eta_n}}. \tag{11}$$

As discussed in previous sections, the ionization energy has been measured to be 87 eV/ion, the kinetic energy of ions leaving the first stage is 12 eV, and the nozzle efficiency is 93%. The remaining free parameter is the second stage coupling efficiency, η_B, which we fit to the data using a least squares algorithm. The semi-empirical fit yielded an ICH coupling efficiency of 74%. In figure 15 we show the resulting comparison. Decreasing E_i and increasing E_1 shifts the curve to the left and increasing η_B and η_n moves the curve upward.

X. Expected Component Efficiency

The overall system efficiency can be estimated for a VASIMR® flight unit based on RF component efficiencies and power consumed by electronics and magnet systems. The first stage and second stage RF generators will be 92% and 98% efficient, respectively, according to the manufacturer Nautel Ltd. The RF transmission system is expected to be 98% efficient. The VX-200 RF transmission systems for both the first and second stages are $96 \pm 0.2\%$ and $96 \pm 0.5\%$, respectively. Those are first generation experimental systems that will be the basis for the expected flight designs. The other primary power consuming system will be the high-temperature superconducting magnet. We have estimated that the magnet power supplies and cryocoolers will consume 500 W and 2 kW, respectively. Other avionics systems should consume less than 300 W. We have decided that these other power loads should be added to the 200 kW used by the RF generators, giving a total power consumption of 202.8 kW. The expected operational values are:

- Helicon generator efficiency (Ideal expected in flight unit): 92%
- ICH generator efficiency (Ideal expected in flight unit): 98%
- Helicon RF transmission efficiency 98%
- ICH RF transmission efficiency 98%
- 100% ionization fraction
- Ionization cost: 87 eV
- Ion kinetic energy out of helicon section: 12 eV
- Nozzle efficiency: 93%

One can see from the above efficiencies and subsystem power losses that the overall efficiency of the VASIMR® will be only a few percent lower than thrust efficiency reported here.

XI. ISS National Laboratory Pathfinder Mission

Ad Astra Rocket Company and the International Space Station (ISS) program are working together to place the VASIMR® engine on a truss of ISS for performance testing. This project is a part NASA's requirement to operate the ISS as a National Laboratory. The VASIMR® flight test will serve as a pathfinder for large, complex science and technology payloads so that NASA better understands integration of such projects. Ad Astra has designated the payload the "Aurora" shown in figure 17. The Aurora will utilize feedback from the attitude control system of the ISS to calculate thrust and performance. The VASIMR® will operate for 15 minutes from large batteries slowly charged by the ISS. The vacuum of space will provide the ultimate test of the VASIMR® engine.

XII. Conclusions and Future Work

For the first time, a thrust efficiency and force of a high-power VASIMR® with good vacuum conditions has been presented. The efficiency was measured to be between 50% and 54% with the specific impulse in the range of 3000 to 3500 s. A maximum force of 4.4 N was measured at 40% thrust efficiency. The ionization cost was determined to be 87 eV for optimized values of RF power and propellant flow rate. A semi-empirical model predicts a thrust efficiency of 64% at 6000 s and 200 kW. The VX-200 has produced a massive amount of new data that is helping narrow the design for a flight unit.

Ad Astra Rocket Company is continuing to study and improve the operation of the VASIMR® engine through testing of the VX-200. We will modify the coupler designs until we can reliably reach 200 kW total power. Recently the vacuum chamber was upgraded for continuous pumping by three cryopanels and a fourth should come on line later this year. The improved vacuum conditions will allow for more accurate measurements of plume properties a few meters downstream. One of the primary experimental goals over the next year will be to demonstrate plasma detachment with detailed measurements of the plasma plume.

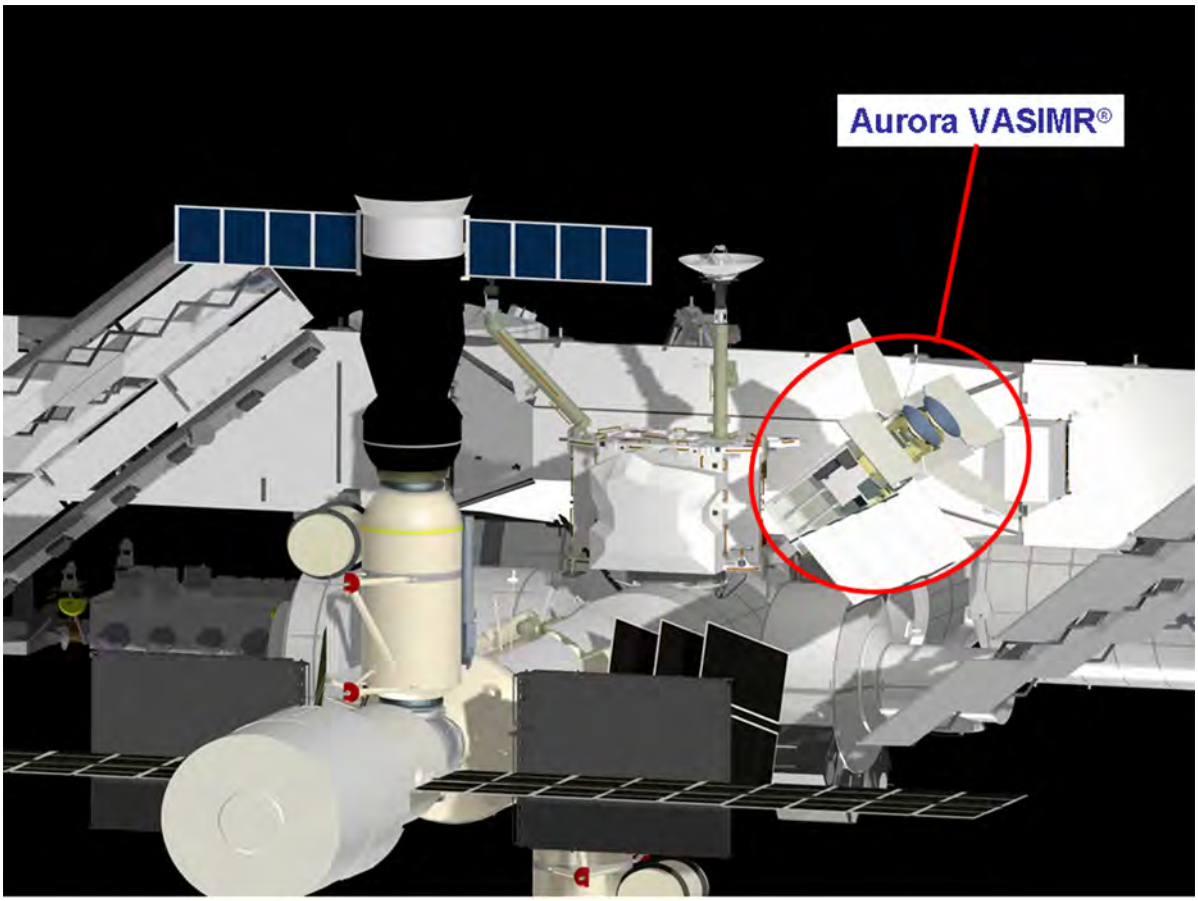

Figure 17. Image of VASIMR® attached to ISS.

References

[1]Frisbee, R., "SP-100 Nuclear Electric Propulsion for Mars Cargo Missions," *29th AIAA/SAE/ASME/ASEE Joint Propulsion Conference*, Monterey, CA, USA, June 1993, AIAA-93-2092.

[2]Frisbee, R., "Electric Propulsion Options for Mars Cargo Missions," *32nd AIAA/ASME/SAE/ASEE Joint Propulsion Conference and Exhibit*, Lake Buena Vista, FL, USA, July 1996, AIAA-96-3173.

[3]Polk, J. and Pivirotto, T., "Alkali Metal Propellants for MPD Thrusters," *AIAA/NASA/OAI Conference on Advanced SEI Technologies*, Cleveland, OH, USA, September 1991, AIAA-91-3572.

[4]Sankaran, K., Cassady, L., Kodys, A., and Choueiri, E., "A Survey of Propulsion Options for Cargo and Piloted Missions to Mars," *Astrodynamics Space Missions and Chaos*, edited by E. Belbruno, D. Folta, and P. Gurfil, Vol. 1017, Annals of the New York Academy of Sciences, New York, NY, USA, 2004, pp. 450–567.

[5]Glover, T., Chang Díaz , F. R., Ilin, A. V., and Vondra, R., "Projected Lunar Cargo Capabilities of High-Power VASIMR Propulsion," *30th International Electric Propulsion Conference*, September 2007, IEPC-2007-244.

[6]Ilin, A., Cassady, L., Glover, T., Carter, M., and Chang Díaz , F., "A Survey of Missions using VASIMR for Flexible Space Exloration," Tech. Rep. JSC-65825, NASA - JSC, April 2010.

[7]Boswell, R. W. and Chen, F. F., "Helicons: The early years," *IEEE Transactions of Plasma Science*, Vol. 25, December 1997, pp. 1229–1244.

[8]Chen, F. F. and Boswell, R. W., "Helicons: The past decade," *IEEE Transactions of Plasma Science*, Vol. 25, December 1997, pp. 1245–1257.

[9]Squire, J. P., Chang Díaz, F. R., Carter, M. D., Cassady, L. D., Chancery, W. J., Glover, T. W., Jacobson, V. J., McCaskill, G. E., Bengtson, R. D., Bering, E. A., and Deline, C. D., "High Power VASIMR Experiments using Deuterium, Neon and Argon," *30th International Electric Propulsion Conference*, September 2007, IEPC-2007-181.

[10]Squire, J., Chang Díaz , F., Glover, T., Carter, M., Cassady, L., Chancery, W., Jacobson, V., McCaskill, G., Olsen, C., Bering, E., Brukardt, M., and Longmier, B., "VASIMR Performance Measurements at Powers Exceeding 50 kW and Lunar Robotic Mission Applications," *International Interdisciplinary Symposium on Gaseous and Liquid Plasmas*, Akiu/Sendai, Japan, September 2008.

[11]Bering, E., Chang Díaz , F., Squire, J., Glover, T., Carter, M., McCaskill, G., Longmier, B., Brukardt, M., Chancery, W., and Jacobson, V., "Observations of single-pass ion cyclotron heating in a trans-sonic flowing plasma," *Physics of Plasmas*, Vol. 17, No. 4, 2010.

[12]Cassady, L., Chancery, W., Longmier, B., Squire, J., Carter, M., Glover, T., Olsen, C., Ilin, A., McCaskill, G., Chang Díaz , F. R., and Bering, E., "VASIMR Technological Advances and First Stage Performance Results," *45th AIAA/ASME/SAE/ASEE Joint Propulsion Conference and Exhibit*, August 2-5 2009, AIAA 2009-5362.

[13]Squire, J., Cassady, L., Chang Díaz, F., Carter, M., Glover, T., Ilin, A., Longmier, B., McCaskill, G., Olsen, C., and Bering, E., "Superconducting 200 kW VASIMR Experiment and Integrated Testing," *Proceedings of the 31st International Electric Propulsion Conference*, Ann Arbor, MI, September 20-24 2009, IEPC-2009-209.

[14]Bering, E., Longmier, B., Chancery, W., Olsen, C., Squire, J., and Chang Díaz, F., "Exhaust plume spatial structure of the VASIMR VX-200," *Proceedings of the 48th AIAA Aerospace Sciences Meeting*, Orlando, FL, January 4-7 2010, AIAA-2009-0622.

[15]Bering, E., Longmier, B., Chang Díaz, F., Squire, J., Glover, T., Chancery, J., Carter, M., Cassady, L., and Brukardt, M., "VASIMR VX-200: High power electric propulsion for space transportation beyond LEO," *Proceedings of AIAA Space 2009 Conference and Exposition*, Pasadena, CA, September 14-17 2009, AIAA-2009-6481.

[16]Longmier, B., Reid, B., Gallimore, A., Chang Díaz, F., Squire, J., Glover, T., Chavers, G., and Bering, E., "Validating a Plasma Momentum Flux Sensor to an Inverted Pendulum Thrust Stand," *Journal of Propulsion and Power*, Vol. 25, No. 3, May-June 2009.

[17]Olsen, C., *Ion Flux Maps and Helicon Source Efficiency in the VASIMR VX-100 Experiment Using a Moving Langmuir Probe Array*, Master's thesis, Rice University, February 2009.

[18]Chavers, D. and Chang-Díaz, F., "Momentum Flux Measuring Instrument for Neutral and Charged Particle Flows," *Review of Scientific Instruments*, Vol. 73, No. 10, 2002.

[19]Longmier, B., Squire, J., Carter, M., Cassady, L., Glover, T., Chancery, W., Olsen, C., Ilin, A., McCaskill, G., Chang Díaz , F. R., and Bering, E., "Ambipolar Ion Acceleration in the Expanding Magnetic Nozzle of the VASIMR VX-200i," *45th AIAA/ASME/SAE/ASEE Joint Propulsion Conference and Exhibit*, August 2-5 2009, AIAA 2009-5359.

[20]Ilin, A., Chang Díaz , F., Squire, J., Tarditi, A., Breizman, B., and Carter, M., "Simulations of Plasma Detachment in VASIMR," *40th AIAA Aerospace Sciences Meeting and Exhibit*, Reno, NV, January 14-17 2002, AIAA 2002-0346.

[21]Arefiev, A. and Breizman, B., "Magnetohydrodynamic scenario of plasma detachment in a magnetic nozzle," *Physics of Plasmas*, Vol. 12, 2005.